Local quantum phase transition in YFe_2Al_{10}

W. J. Gannon[a,1], L. S. Wu[b,2], I. A. Zaliznyak[c], W. H. Xu[c], A. M. Tsvelik[c], Y. Qiu[d], J. A. Rodriguez-Rivera[d,e], and M. C. Aronson[a]

[a]Department of Physics and Astronomy, Texas A&M University, College Station, TX 77843-4242; [b]Neutron Scattering Division, Oak Ridge National Laboratory, Oak Ridge, TN 37831; [c]Condensed Matter Physics and Materials Science Division, Brookhaven National Laboratory, Upton, NY 11973; [d]National Institute of Standards and Technology Center for Neutron Research, National Institute of Standards and Technology, Gaithersburg, MD 20899; and [e]Department of Materials Science and Engineering, University of Maryland, College Park, MD 20740

Edited by Subir Sachdev, Harvard University, Cambridge, MA, and approved May 9, 2018 (received for review December 13, 2017)

A phase transition occurs when correlated regions of a new phase grow to span the system and the fluctuations within the correlated regions become long lived. Here, we present neutron scattering measurements showing that this conventional picture must be replaced in YFe_2Al_{10}, a compound that forms naturally very close to a $T = 0$ quantum phase transition. Fully quantum mechanical fluctuations of localized moments are found to diverge at low energies and temperatures; however, the fluctuating moments are entirely without spatial correlations. Zero temperature order in YFe_2Al_{10} is achieved by an entirely local type of quantum phase transition that may originate with the creation of the moments themselves.

magnetism | quantum matter | neutron scattering

Magnetic order arises from the growth of magnetic correlations, which become increasingly long lived and extend over longer distances as the phase transition to magnetic order is approached. The magnetically ordered ground state can be destabilized by pressure, composition, or magnetic field, and there are extremal values of these nonthermal variables where order occurs only at $T = 0$, the Quantum Critical Point (QCP). It is the strong quantum fluctuations associated with low dimensionality or alternatively, the frustration of competing interactions on lattices with certain geometries that can suppress magnetically ordered phases to produce these QCPs. Magnetic order also requires magnetic moments, which in metals, can be produced by different types of $T = 0$ instabilities. For spatially localized f electrons, it is the Kondo compensation provided by conduction electrons that determines whether a moment is retained at $T = 0$. Mott physics governs the more delocalized d electrons, where correlations among the mobile electrons may produce a spatially localized moment with a magnitude that can approach the large moments possible in insulators or alternatively, correlations so weak that they cannot induce even a tiny moment that could lead to magnetic order at a correspondingly low but still nonzero temperature. Phase transitions leading to moment formation at $T = 0$ are expected to have a very different character than those that lead only to magnetic order.

It has proven difficult to make a clean experimental distinction between QCPs that are related to magnetic order, involving a broken symmetry, and those that correspond to moment formation. The conventional picture of classical phase transitions can be extended in certain systems to $T = 0$, where neutron scattering documents the growth of spatial and temporal correlations that are related to fluctuations of the order parameter (1, 2). Only mean field behavior (3–5) is observed, indicating that these systems lack strong quantum fluctuations. In contrast, neutron scattering experiments on $CeCu_{6-x_C}Au_{x_C}$ (6) and $BaFe_{1.85}Co_{0.15}As_2$ (7, 8) find strong quantum critical (QC) fluctuations and the breakdown of conventional Fermi liquid (FL) behavior near the wave vectors that will eventually become magnetic Bragg peaks in nearby antiferromagnetic (AF) phases. So far, there is no case where the comparison of experimental and theoretical QC phenomena definitively identifies QC fluctuations of a $T = 0$ order parameter of any kind (9). Nonetheless, there is mounting evidence that moment formation may play an important role near QCPs. In the Kondo breakdown scenario proposed for f electron heavy fermion compounds, the QC fluctuations associated with magnetic order are strong enough to localize a moment-bearing electron (10, 11). The collapse of the Kondo effect may occur exactly at a magnetic QCP (12) or simply close to one (13, 14). It is accompanied not by QC order parameter fluctuations, as near a $T = 0$ magnetic phase transition, but rather, by QC fluctuations between two Fermi surfaces, one containing the electron that will be localized and one that does not. A very different $T = 0$ phase transition envisages moment formation as the consequence of a topological instability in a metal with strong electronic correlations (15, 16). In both of these cases, it is the dynamics of individual moments that is QC, and the intersite interactions that would otherwise lead to spatial correlations are presumed to be much weaker. Particularly appropriate for d electron-based metals, the orbital selective Mott transition (OSMT) provides a general theoretical structure (17) for a phase transition where one or more orbitals can transition from being localized and magnetic to delocalized and nonmagnetic (18–20). Practically speaking, the emergence of a magnetic moment in a metal, either by a topological instability or by Mott physics, is very likely to lead to magnetic order, except in the most frustrated of systems. Magnetic phase transitions at $T = 0$ do not require simultaneous moment formation via electronic localization transitions; however, we lack direct experimental evidence of the converse situation, where an

Significance

We report the discovery of a type of phase transition that occurs at $T = 0$. In continuous phase transitions, order occurs when the size and lifetime of small ordered regions increase until they span the system and become static. Reported here is experimental evidence of a transition where this paradigm fails. Our observed phase transition is local, where each magnetic moment in YFe_2Al_{10} is independent of every other moment, yet each moment follows the same spectrum of quantum critical fluctuations. The phase transition present in YFe_2Al_{10} is a realization of a scenario only hinted at by theory, corresponding to the formation of magnetic moments, with no evidence for the breaking of translational symmetry that accompanies magnetic order.

Author contributions: W.J.G., L.S.W., and M.C.A. designed research; W.J.G., L.S.W., I.A.Z., W.H.X., A.M.T., Y.Q., J.A.R.-R., and M.C.A. performed research; W.J.G. analyzed data; and W.J.G., L.S.W., I.A.Z., W.H.X., A.M.T., Y.Q., J.A.R.-R., and M.C.A. wrote the paper.

The authors declare no conflict of interest.

This article is a PNAS Direct Submission.

[1]To whom correspondence should be addressed. Email: wgannon@physics.tamu.edu.

[2]Department of Physics, South University of Science and Technology of China, Shenzhen, 518055, China.

This article contains supporting information online at www.pnas.org/lookup/suppl/doi:10.1073/pnas.1721493115/-/DCSupplemental.

Published online June 18, 2018.

electronic localization transition leading to moment formation can exist independent of magnetic order. It is significant that the neutron scattering results reported here show that YFe_2Al_{10} is an example of a metal on the verge of moment formation but without any vestige of magnetic order (21, 22).

In materials that are magnetically ordered or nearly so, magnetic correlations depend strongly on wave vectors $\boldsymbol{q}$ that reflect the spatial periodicity of the magnetic structure. Our inelastic neutron scattering measurements show (Fig. 1 *A* and *B*) that the magnetic fluctuations in YFe_2Al_{10} are very different. Here, the scattered intensity $I(\boldsymbol{q})$ is dominated by a broad ridge of scattering along wave vectors $\boldsymbol{q}$ parallel to [0, 0, L], lying in the critical ac plane defined by the Fe layers (Fig. 1*D*, *Inset* and *SI Appendix*) (21, 23, 24). Consistent with the $T/B^{0.6}$ scaling observed in the magnetization and specific heat (25), the scattering is strongly suppressed by magnetic fields B (Fig. 1*A*). The critical part of $I(\boldsymbol{q})$ can be exposed by using similar data obtained at 9 T (Fig. 1*A*, *Right*) as an improvised background for the $B = 0$ data (Fig. 1*A*, *Left*). Fig. 1*B* shows that the result is a weak and broad modulation of the field-dependent component of the scattering in the [0, K, 0] direction $I(q_K)$ perpendicular to the Fe layers, with a breadth that extends over more than the full Brillioun zone.

The neutron intensity $I(\boldsymbol{q}, E)$ is the product of the magnetic form factor $F^2(\boldsymbol{q})$, reflecting the spatial distribution of magnetization clouds associated with the fluctuating moments, and the structure factor $S(\boldsymbol{q}, E)$, which probes correlations among moments. The latter can be isolated (Fig. 1 *C* and *D*) by comparing $I(q_K, E)$ with both the isotropic Fe^{2+} atomic form factor (26) and the form factor $F^2_{xz,yz}(q_K)$ of the Fe $d_{xz,yz}$ Wannier orbitals obtained from a tight binding band structure calculation (*SI Appendix*). $I(q_K)$ falls off more quickly than the Fe^{2+} atomic form factor, implying a minimal degree of Fe moment delocalization in YFe_2Al_{10} that is well-captured by the calculations. Unlike the spherically symmetric Fe^{2+} atomic form factor, $I(0, q_K, q_L)$ is strikingly anisotropic, and the dominance near the Fermi level of $d_{xz,yz}$ orbitals provides a natural explanation (*SI Appendix*, Fig. S3). After the computed form factor is removed from the measured intensity $I(q_K, E) = F^2_{xz,yz}(q_K)S(E)$, there is no further wave vector dependence of the structure factor, which is solely a function of energy E, $S(\boldsymbol{q}, E) = S(E)$ (Fig. 1*D*). Since an atomic energy scale $\sim$1 eV controls the spatial distribution of the moment density in the d_{xz} orbital that is reflected in the form factor, the wave vector modulation of $I(q_K)$ is correspondingly unaffected by temperatures from 0.07 to 20 K, magnetic fields as large as 9 T, and excitation energies from $0.35 - 1.5$ meV (*SI Appendix*, Fig. S6). Remarkably, the moments in YFe_2Al_{10} are highly localized in space and fluctuate independently, with no sign of the spatial correlations that are a foundational element of conventional phase transitions and their $T = 0$ analogs.

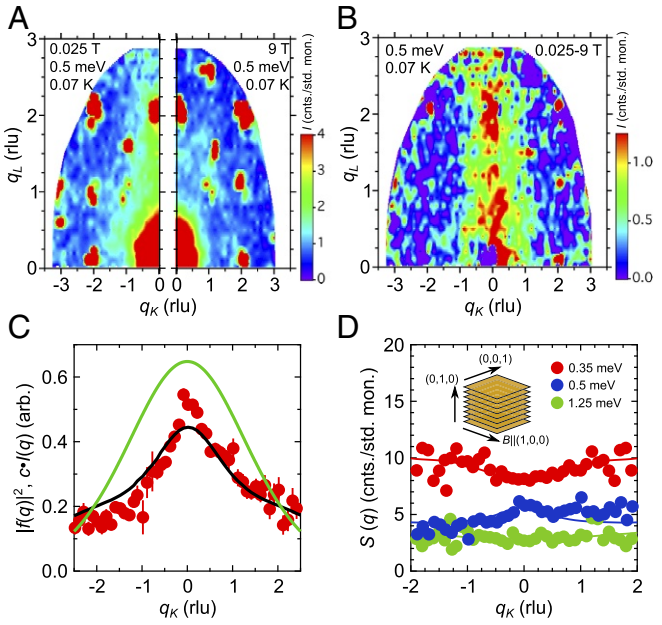

Fig. 1. Spatially localized magnetic fluctuations in YFe_2Al_{10}. (*A*) The intensity of neutrons scattered with energy transfer 0.5 meV in the [0, *K*, *L*] plane at 0.07 K in fields of 0.025 *T* (*Left*) and 9 *T* (*Right*) and their difference *I*(0 *T*) − *I*(9 *T*) (*B*). The tails of nuclear Bragg peaks are clearly observed in *A* at integer values of *K* and *L*. A diffuse ridge of scattering is evident along [0, 0, *L*] at $q_K = 0$ rlu. Data are monitor normalized. (*C*) Wave vector q_K dependence of the q_L integrated intensity $I(q_K)$ is better described by the YFe_2Al_{10} magnetic form factor $F^2_{xz,yz}(q_K)$ from electronic structure calculations (black line) (*SI Appendix*) than isotropic Fe^{2+} form factor (green line) (26). Both form factors are scaled to the data. Strong anisotropy in the intensity indicates that $d_{xz,yz}$ orbitals dominate. (*D*) The $T = 0.07$ K structure factor $S(q_K)$ is isolated for different fixed energies by dividing $I(q_K)$ by $F^2_{xz,yz}(q_K)$. Solid lines are obtained by fitting $I(q_K)$ to a Lorentzian and dividing by the computed $F^2_{xz,yz}(q_K)$, showing that $S(q_K)$ is independent of wave vector q_K. (*Inset*) The correspondence between the scattering wave vectors q_K and q_L and the *ac* planes containing the nearly square Fe nets in YFe_2Al_{10}. The magnetic field is oriented in the critical *ac* plane along the (100) direction. All data were measured on MACS (46). Error bars in each figure represent 1 SD.

Despite the absence of spatial correlations among the fluctuating moments in YFe_2Al_{10}, their dynamics are manifestly QC, with the strongest scattering associated with fluctuations having the lowest energies or longest lifetimes. Inelastic neutron scattering experiments (Fig. 2*A*) reveal a gapless spectrum of excitations, where the structure factor $S(E)$, obtained from the data in Fig. 1 by integrating over q_K (*SI Appendix*), is expressed in terms of the magnetization squared M^2. The critical behavior of the energy dependence is determined by plotting the inverse of $M^2 - C$, where C is a small and energy-independent contribution to the moment, as a function of E^{Δ}, and within their accuracy, the neutron scattering data are consistent with $\Delta = 1.4$, which is the power law exponent that was previously reported for the temperature divergence of the magnetic susceptibility $\chi(T) \propto T^{-1.4}$. The QC dynamics are a continuum that extends to the lowest energies probed in this experiment (Fig. 2*B*). Since M^2 must remain finite, the QC energy dependence $S(E) \sim E^{-1.4}$ cannot extend to $E \to 0$. The local QC behavior reported here is likely a high-temperature phenomenon, and it will be cut off at lower temperatures either by residual interactions that lead to ordered states, like magnetic order or superconductivity, or perhaps, by interactions within the ordered lattice of Fe moments that lead to a coherent ground state as in a Kondo lattice. By expressing M^2 in absolute units, we see that the fluctuating local moments responsible for the scattering in the energy window of our experiment from 0.35 to 1.5 meV have magnitudes of $\sim 0.3 - 0.4\ \mu_B$/Fe, similar to the local moment magnitude deduced from fitting the Curie–Weiss law to the static susceptibility $\chi_0(T)$ in the temperature range $100 - 750$ K (21). The energy-independent scattering C likely reflects the presence of a broad and weakly correlated band of quasiparticle excitations as implied by the modest Pauli susceptibility and Sommerfeld coefficient reported for YFe_2Al_{10} (21). The breadth of this band is estimated as ~ 0.7 eV (Fig. 2*A*), which is the energy where the integral of the fit to the experimental data reaches the square of the full spin $S = 2$ Fe^{2+} moment $M^2 = 24\ \mu_B^2$.

Conventionally, proximity to a phase transition results in the transfer of spectral weight to lower energies. Something very different occurs in YFe_2Al_{10}, where the q_L integrated scattering $I(q_K, E)$ (Fig. 3*A*) as well as the associated $S(E)$ (Fig. 3*B*) are constant over almost three decades of temperature from 0.07 to 20 K. This simple observation has remarkable consequences. Namely, the principle of detailed balance gives $S(E, T) \sim \chi''(E, T)/(1 - exp(-E/k_B T))$, where k_B is

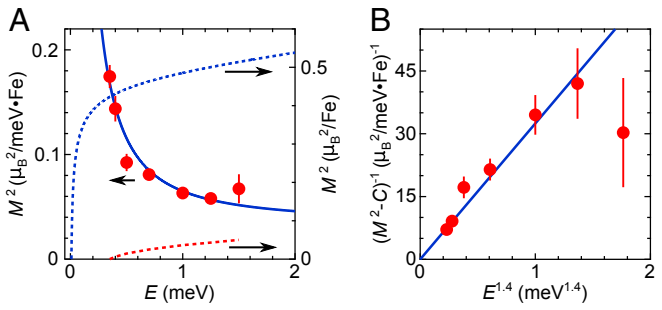

Fig. 2. A quantum continuum in YFe_2Al_{10}. (*A*) The energy dependence of the magnetization squared M^2 of the fluctuating moments in YFe_2Al_{10} at 0.07 K and $B = 0.025$ *T*. Details of the normalization are in *SI Appendix*. The solid blue line is a fit to the data where $M^2(E) = C + aE^{-1.4}$, with $C = 0.034\ \mu_B^2/\text{meV}\cdot\text{Fe}$. The dashed red line is the integral over the measured QC fluctuations $aE^{-1.4}$, while the dashed blue line represents the integral over the power law fit to $M^2(E)$ for $E > k_BT$. (*B*) The inverse of $M^2 - C$ is plotted as a function of $E^{1.4}$. The blue line indicates the best linear fit. Error bars in both figures represent 1 SD.

Boltzmann's constant. The detailed balance factor $(1 - exp(-E/k_BT))$ is manifestly a function of E/k_BT, and thus, the imaginary part of the dynamical susceptibility $\chi''(E, T)$ must also be a function of E/k_BT that cancels the temperature dependence of the detailed balance factor. QC fluctuations having no energy scale other than temperature itself are the hallmark of QC phase transitions (6–8, 27–32), and Fig. 3*C* shows that $\chi'' = \chi''(E/T)$ in YFe_2Al_{10} as well. Because our measurements in YFe_2Al_{10} are carried out over such a broad range of energies and temperatures, it is also possible to show that these data collapse onto a single universal curve by plotting $\chi''T^{1.4}$ as a function of (E/k_BT) (Fig. 3*D*), where the universal curve is well-reproduced by the expression $\chi''(E, T)T^{1.4} \propto x^{-\Delta}\tanh(x)$, with $\Delta = 1.4$. In previously investigated systems, the E/T scaling is always associated with the collapse of magnetic order, and it is only observed over a limited range of wave vectors that are associated with incipient magnetic order. In contrast, the E/T scaling of χ'' in YFe_2Al_{10} extends over the entire range of wave vectors accessed in this experiment, amounting to more than an entire Brillouin zone.

The energy and temperature dependencies of χ'' provide the needed connection between the neutron scattering measurements and the previously reported temperature dependence of the static susceptibility $\chi_0(T) \sim T^{-1.4}$ (25), since the Kramers–Kronig relation gives

$$\chi_0(T) = \int dE\ \chi''(E, T)/E = T^{-\Delta}\int dx\ \tanh(x)/x^{1+\Delta}, \quad [1]$$

where $\chi''E^{1.4} \propto \tanh(x)$ and $x = E/k_BT$. Agreement between these two independent determinations of $\chi_0(T)$ requires that $\Delta = 1.4$, a value that is wholly within the experimental bounds of the neutron scattering experiment (Fig. 2*B*). In addition, the integral itself must remain finite. The strong divergence of $\chi''(E)$ implies that it cannot extend to arbitrarily low energies and temperatures, and a proposal for a particular energy and temperature cutoff is compared with the scaled data in *SI Appendix*. For the range of temperatures and energies accessed in our experiments, the matching energy and temperature dependencies of the neutron scattering and magnetic susceptibility measurements imply that both measurements probe the same QC fluctuations. It is worth pointing out that the strong energy and temperature divergences of χ_0 and χ'' are inconsistent with an appreciable role for disorder in the QC behavior of YFe_2Al_{10} (33–37).

The structure, symmetries, and interactions present in a given material determine the conditions under which a $T = 0$ phase transition may occur, and therefore, modifications to these quantities via pressure, stress, or composition will affect the tendency to order. Increasing temperature weakens QC fluctuations as would magnetic fields if the QCP corresponds to the onset of magnetism. Scaling analyses of the static susceptibility $\chi_0 \sim T^{-1.4}f(T/B^{0.6})$ have shown that a single variable $T/B^{0.6}$ controls the QC fluctuations for a wide range of fields and temperatures in YFe_2Al_{10} (25). Is $T/B^{0.6}$ observed as well in the dynamical susceptibility? Fig. 4*A* shows that the dynamical susceptibility has an evocative field dependence at $T = 0.07$ K, $\chi'' \sim [A + bB^{0.6}]^{-1}$ with $A = 3.65\ \text{meV}\cdot\text{Fe}/\mu_B^2$, and $b = 0.19\ T^{-0.6}\text{meV}\cdot\text{Fe}/\mu_B^2$, suggesting a possible link to the field dependencies observed in YFe_2Al_{10} in the magnetization and specific heat at the lowest temperatures. A particularly simple formulation of χ'' was previously proposed in the benchmark QC system $CeCu_{6-x}Au_x$, where the energy and temperature dependencies of χ'' could be separated from the field dependence (6). Specifically, the divergence in the generalized susceptibility χ would only occur if E, T, and B approach zero; otherwise, the largest of the thermal, Zeeman, or measurement energy serves to cut off the divergence. The simplest case (Fig. 2*B*) takes $B = 0$ and $T = 0.07$ K, where the energy

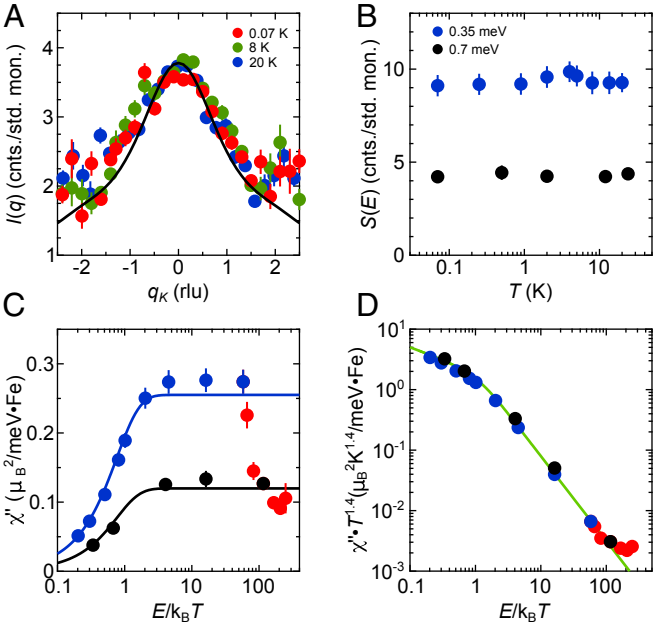

Fig. 3. *E/T* scaling of the magnetic dynamics in YFe_2Al_{10}. (*A*) The q_L integrated scattering $I(q_K)$ for an energy transfer of 0.35 meV is presented at temperatures 0.07 K (red circles), 8 K (green circles), and 20 K (blue circles). The black line is the scaled computed form factor $F^2_{xz,yz}(q_K)$. (*B*). $S(E)$ is obtained by integrating $S(\mathbf{q}, E)$ over experimental values of the wave vectors q_L and q_K. Within the accuracy of our measurements, $S(E)$ is independent of temperatures in the range from 0.07 to 24 K for the fixed energies $E = 0.35$ meV (blue circles) and $E = 0.7$ meV (black circles). (*C*) The principle of detailed balance, $\chi''(E, T) \sim S(E, T)\ (1 - exp(-E/k_BT)$, is used to relate $S(E, T)$ to the imaginary part of the dynamical susceptibility $\chi''(E, T)$, which has also been integrated over these same wave vectors. $\chi''(E, T)$ is plotted at different temperatures from 0.07 to 24 K for energy transfers of 0.35 meV (blue circles) and 0.7 meV (black circles) and for a range of different energy transfers from 0.35 to 1.5 meV at 0.07 K (red circles). The solid lines are fits to the expression $\chi'' \propto \tanh(x)$, where $x = E/k_BT$. (*D*) The data in *C* can be collapsed onto a single universal curve when $\chi''T^{1.4}$ is plotted as a function of E/k_BT. The solid green line compares the scaled data $\chi''T^{1.4}$ with the function $x^{-\Delta}\tanh(x)$, where $x = E/k_BT$ and $\Delta = 1.4$. Error bars in each figure represent 1 SD.

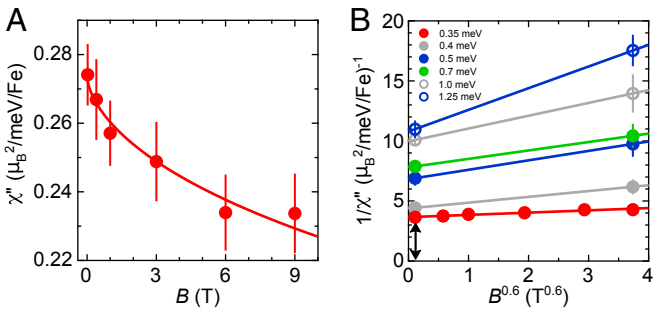

Fig. 4. Magnetic fields and the Quantum Critical Scaling of the dynamics in YFe_2Al_{10}. (*A*) The field dependence of χ'', measured at $T = 0.07$ K, with an energy transfer $E = 0.35$ meV. The solid line is a fit to the expression $\chi'' \sim A + bB^{-0.6}$, with $A = 3.62$ meV $\cdot$ Fe/μ_B^2 and $b = 0.19$ $T^{-0.6}$ meB $\cdot$ Fe/μ_B^2. (*B*) The inverse of χ'' plotted as a function of $B^{0.6}$ for $T = 0.07$ K at different fixed energy transfers as indicated. Error bars represent 1 SD.

dependence dominates and gives $1/\left(\chi'' - \tilde{C}\right) = \tilde{a}E^{1.4}$, with $\tilde{C} = 0.053\ \mu_B^2/\text{meV} \cdot Fe$ providing a scale for the fine tuning needed to drive YFe_2Al_{10} exactly to the QCP. These neutron scattering experiments directly probe the response to the fluctuating fields associated with the QCP in YFe_2Al_{10} for energies that are, for the most part, larger than the thermal energy $k_B T$ and the Zeeman energy $g\mu_B B$. The inverse of χ'' is plotted as a function of $B^{0.6}$ at different fixed energy transfers in Fig. 4*B*. The $B = 0$ intercept of $1/\chi''$ decreases with decreasing energy, consistent with an energy dependent cutoff. However, the slope of the $B^{0.6}$ dependence is also energy dependent, proving that the energy and field dependencies of χ'' are significantly intertwined and cannot be readily separated, even when energy provides the largest scale. Still, it is reasonable to expect that the $T/B^{0.6}$ scaling found in $\chi_0(T)$ is most likely to be observed in χ'' when the excitation energy E is small compared with the thermal and magnetic field scales, a regime that is largely unaddressed in our neutron scattering measurements.

The previously reported scaling analysis made it clear that YFe_2Al_{10} is naturally located by its composition to be very close to a $T = 0$ phase transition. The neutron scattering measurements reported here reveal that this phase transition is highly unconventional. Specifically, the near divergence of $S(E)$ as $E \to 0$ shows that QC magnetic fluctuations with a timescale ξ_τ dominate at the low energies probed in these experiments, while spatial correlations ξ_r among these moments are absent. This violates the foundational property of conventional phase transitions (38), where ξ_r and ξ_τ are related by the dynamic exponent z, $\xi_r^z = \xi_\tau$. An intriguing alternative has recently been suggested, where a topological phase transition could produce anomalously weak spatial correlations as well as reproduce several of the experimental findings in YFe_2Al_{10} (39, 40).

Our major finding is that the excitations detected by our neutron scattering measurements in YFe_2Al_{10} are those of individual and highly localized magnetic moments, each fluctuating independently with the same anomalous spectrum, without any evidence for a nearby broken symmetry. The low-temperature divergences of quantities, like the magnetic susceptibility, the specific heat, and the electrical resistivity, all attest to the breakdown of normal metallic behavior, which we now know occurs in the absence of magnetic order at temperatures as low as 0.07 K. The observation of E/T scaling in the neutron scattering measurements indicates that the magnetic excitations are fundamentally modified relative to the damped spin waves or the continuum of single-particle excitations that are expected near a classical magnetic phase transition.

The small but localized moments identified by both the Curie–Weiss susceptibility and the neutron scattering measurements imply that YFe_2Al_{10} forms very close to an electronic localization transition. As was shown in both Fe and Mn pnictides and chalcogenides (41–43), such moments result from Hunds and Coulomb interactions that provide electronic correlations that are potentially strong enough to localize one or more Fe d orbitals in YFe_2Al_{10}. Since the localized moments emerge from a relatively flat band (*SI Appendix*, Fig. S3), it is likely that the form factor of the moments, which encodes the orbital content, will dominate the $\boldsymbol{q}$ dependence of the scattering, just as we have observed. The stabilization of the Fe moments is envisaged as a continuous cross-over or transition between a coherent metallic state where the localized moments are wholly quenched and a state where this compensation has failed, leading to incoherent and localized magnetic moments (41). A Mott-like transition could ensue at $T = 0$ for a critical interaction strength accompanied by QC fluctuations between these two topologically distinct states that are degenerate at the QCP. The comparison of the measured and computed form factors suggests that it is the $d_{xz,yz}$ orbitals that are most localized in YFe_2Al_{10}, while the other orbitals are represented as delocalized and weakly correlated electronic states that result in the overall metallic character of YFe_2Al_{10}, evident from the temperature dependence of the electrical resistivity as well as the modest Pauli susceptibility and Sommerfeld constant. Consequently, it seems possible that YFe_2Al_{10} is very close to an OSMT (17–20) and that it is QC fluctuations between these phases at $T = 0$ that lead to the non-FL properties of YFe_2Al_{10}. Detailed investigations of the Fermi surface in YFe_2Al_{10}, ideally as pressure or another nonthermal parameter tunes the localized moments to extinction, will be required to further evaluate this proposal.

For now, the nature of the $T = 0$ phase transition that drives the quantum critical behavior that is so dominant in YFe_2Al_{10} remains unknown, although its consequences are transformative. Neutron scattering provides a powerful and direct means to show that this phase transition is not of the conventional Landau–Ginsburg–Wilson type. Unlike previously studied systems, where similar measurements found that QC behavior was never wholly free of the magnetic correlations associated with proximate magnetic order, the complete absence of these correlations in YFe_2Al_{10} indicates that here the QCP stands alone and is definitively of a type that has never been observed before. YFe_2Al_{10} is almost unique in that no fine tuning is required to access its QCP, which affects a remarkably broad range of temperatures and fields. In this sense, it might be considered the d-electron analog of $\beta - YbAlB_4$ (44, 45). Since no bulky pressure apparatus and no potentially disruptive disorder from compositional variation are necessary in YFe_2Al_{10} to fine tune the QCP, our results open the door for further explorations of the nature and properties of this quantum phase transition using the most powerful spectroscopic and imaging tools at our disposal.

Materials and Methods

Samples and Experimental Setup. To measure the excitation spectrum of YFe_2Al_{10}, neutron scattering measurements were carried out in the 0, q_K, q_L scattering plane on the Multi Axis Crystal Spectrometer (MACS) instrument at the Center for Neutron Research at the National Institute of Standards and Technology (46). Apart from a small orthorhombic distortion in the ac basal plane, we would expect to find similar data in the (nearly) equivalent q_H, q_K, 0 scattering plane. The sample consisted of two coaligned single crystals of YFe_2Al_{10} with a total mass of 2 g mounted in a dilution refrigerator equipped with a superconducting magnet with an 11-T vertical field aligned with the (100) crystal direction. To reduce background scattering in the double-focusing mode, we used a 3.3 × 7.7-cm beam mask to focus the neutron beam on the 1.5 × 2.5-cm sample. For all measurements, a small bias field of about 0.025 *T* was used, suppressing superconductivity of the aluminum sample holder at low temperatures and for consistency at temperatures above T_c of aluminum, 1.2 K. Undesired background scattering was eliminated by setting the dark angle of the magnet at 90°

away from the (010) direction and using final neutron energy E_f = 3.0 and 3.7 meV ($\lambda_f = 5.22$ and 4.70 Å, respectively). Be filters were used between the neutron source and the sample, while Be (for $E_f = 3.0$ meV) or BeO (for $E_f = 3.7$ meV) filters were used between the sample and detector. All reciprocal lattice vectors are indexed as (q_H q_K q_L), with reciprocal lattice units $q_K = 2\pi/b = 0.62$ Å^{-1} and $q_L = 2\pi/c = 0.70$ Å^{-1}.

Data Analysis. The quantities of interest determined in our neutron scattering measurements at a given wave vector $\boldsymbol{q}$ and energy E are the magnetic structure factor $S(\boldsymbol{q}, E)$ and the imaginary part of the magnetic susceptibility $\chi''(\boldsymbol{q}, E)$. Both relate to our measured neutron scattering intensity $I(\boldsymbol{q}, E)$ in a straightforward way (47). $S(\boldsymbol{q}, E)$ is determined by dividing $I(\boldsymbol{q}, E)$ by the square of the magnetic form factor $F^2(\boldsymbol{q})$, $S(\boldsymbol{q}, E) \sim I(\boldsymbol{q}, E)/F^2(\boldsymbol{q})$, while $\chi''(\boldsymbol{q}, E)$ is related to $S(\boldsymbol{q}, E)$ by the principle of detailed balance, where $\chi''(\boldsymbol{q}, E) \sim S(\boldsymbol{q}, E)\left(1 - e^{-E/k_B T}\right)$ for a given temperature T.

Our measurements on the MACS instrument at the Center for Neutron Research at the National Institute of Standards and Technology (46) (Fig. 1*A* has an example of the data) acquire the $\boldsymbol{q}$ dependence of the scattered neutron intensity at different fixed energy transfers, temperatures, and magnetic fields in the $\boldsymbol{q}$= [0, *K*, *L*] plane (the q_K–q_L plane). After normalizing the measured intensity by the incident neutron flux, areas of $\boldsymbol{q}$ space contaminated by tails from Bragg reflections were masked. The results were integrated (i.e., numerically summed) along the q_L direction over the range *L* = [0.8, 1.8] reciprocal lattice units (rlu) and were then normalized by that range of q_L, Δq_L, which covers one full Brillouin Zone. This zone was selected to minimize possible contamination from the direct beam. This procedure yields the q_K dependence of our measured intensity, $I(q_K, E)$,

$$I(q_K, E) = \int_{0.8\ \text{rlu}}^{1.8\ \text{rlu}} I(q_K, q_L, E)\,dq_L/\Delta q_L. \quad [2]$$

Examples of $I(q_K, E)$ are given in Figs. 1*C*, 3*A*, and 4*A* and *SI Appendix*, Fig. S6. $I(E)$ can be obtained with a similar integration of the q_K dependence. $S(\boldsymbol{q}, E)$ and $S(E)$ are obtained from these quantities after accounting for the form factor, which is described in *SI Appendix*.

ACKNOWLEDGMENTS. The authors acknowledge useful discussions with C. Varma, E. Abrahams, D. MacLaughlin, L. Shu, S. Chakravarty, G. Aeppli, S. Raymond, and C. Broholm. Part of this research was conducted at Brookhaven National Laboratory, where W.J.G., L.S.W., and M.C.A were supported under the auspices of US Department of Energy, Office of Basic Energy Sciences Contract DE-AC02-98CH1886. I.A.Z., W.H.X., and A.M.T. have been separately supported under the auspices of US Department of Energy, Office of Basic Energy Sciences Contract DE-SC0012704. W.H.X. was supported by the Center for Computational Design of Functional Strongly Correlated Materials and Theoretical Spectroscopy under US Department of Energy Grant DE-FOA-0001276. Part of this work was performed at the Aspen Center for Physics, which is supported by National Science Foundation Grant PHY-1066293. Access to the MACS was provided by the Center for High Resolution Neutron Scattering, a partnership between the National Institute of Standards and Technology and the National Science Foundation under Agreement DMR-1508249.

1. Knafo W, Raymond S, Lejay P, Floquet J (2009) Antiferromagnetic criticality at a heavy-fermion quantum phase transition. *Nat Phys* 5:753–757.
2. Singh DK, et al. (2011) Field-induced quantum fluctuations in the heavy-fermion superconductor $CeCu_2Ge_2$. *Sci Rep* 1:117.
3. Hertz JA (1976) Quantum critical phenomena. *Phys Rev B* 14:1165.
4. Moriya T (1985) *Spin Fluctuations in Itinerant Electron Magnetism*, Springer Series in Solid-State Sciences (Springer, Berlin), Vol 56.
5. Millis JA (1993) Effect of a nonzero temperature on quantum critical points in itinerant fermion systems. *Phys Rev B* 48:7183–7196.
6. Schroeder A, et al. (2000) Onset of antiferromagnetism in heavy-fermion metals. *Nature* 407:351–355.
7. Inosov DS, et al. (2010) Normal-state spin dynamics and temperature-dependent spin-resonance energy in optimally doped $BaFe_{1.85}Co_{0.15}$ As_2. *Nat Phys* 6:178–181.
8. Varma CM, Zhu L, Schroder A (2015) Quantum critical response function in quasi-two-dimensional itinerant antiferromagnets. *Phys Rev B* 92:155150.
9. Sachdev S (2008) Quantum magnetism and criticality. *Nat Phys* 4:173–185.
10. Coleman P, Pépin C, Si Q, Ramazashvili R (2001) How do Fermi liquids get heavy and die? *J Phys Condens Matter* 13:R723–R738.
11. Si Q, Rabello S, Ingersent K, Smith JL (2001) Locally critical quantum phase transitions in strongly correlated metals. *Nature* 413:804–808.
12. Paschen S, et al. (2004) Hall-effect evolution across a heavy-fermion quantum critical point. *Nature* 432:881–885.
13. Friedemann S, et al. (2009) Detaching the antiferromagnetic quantum critical point from the Fermi - surface reconstruction in $YbRh_2Si_2$. *Nat Phys* 5:465–469.
14. Custers J, et al. (2010) Evidence for a non-Fermi liquid phase in Ge-substituted $YbRh_2Si_2$. *Phys Rev Lett* 104:186402.
15. Senthil T, Vojta M, Sachdev S (2004) Weak magnetism and non-Fermi liquids near heavy-fermion critical points. *Phys Rev B* 69:035111.
16. Senthil T (2008) Critical Fermi surfaces and non-Fermi liquid metals. *Phys Rev B* 78:035103.
17. Vojta M (2010) Orbital-selective Mott transitions: Heavy fermions and beyond. *J Low Temp Phys* 161:203–232.
18. Anisimov VI, Nakrasov IA, Kondakov DE, Rice TM, Sigrist M (2002) Orbital-selective Mott-insulator transition in $Ca_{2-x}Sr_xRuO_4$. *Eur Phys J B* 25:191–201.
19. de' Medici L, Georges A, Kotliar G, Biermann S (2005) Mott transition and Kondo screening in f-electron metals. *Phys Rev Lett* 95:066402.
20. de' Medici L, Hassan SR, Capone M, Dai X (2009) Orbital-selective Mott transition out of band degeneracy. *Phys Rev Lett* 102:126401.
21. Park K, et al. (2011) Field-tuned Fermi liquid in quantum critical YFe_2Al_{10}. *Phys Rev B* 84:094425.
22. Huang K, et al. (2018) Anomalous quantum-critical spin dynamics in YFe_2Al_{10}. *Phys Rev B* 97:155110
23. Thiede VMT, Ebel T, Jeitschko W (1998) Ternary aluminides LnT_2Al_{10} (Ln=Y,La-Nd,Sm,Gd-Lu and T=Fe,Ru,Os) with $YbFe_2Al_{10}$ type structure and magnetic properties of the iron-containing series. *J Mater Chem* 8:125–130.
24. Kerkau A, et al. (2012) Crystal structure of yttrium iron aluminium (1/2/10), YFe_2Al_{10}. *Z Kristallogr New Cryst Struct* 227:289–290.
25. Wu LS, Kim MS, Park K, Tsvelik AM, Aronson MC (2014) Quantum critical fluctuations in layered YFe_2Al_{10}. *Proc Natl Acad Sci USA* 111:14088–14093.
26. Brown PJ (2006) Magnetic form factors. *International Tables for Crystallography*, ed Prince E (Wiley, Hoboken, NJ), Vol C, pp 454–461.
27. Varma CM, Littlewood PB, Schmitt-Rink S (1989) Phenomenology of the normal state of Cu-O high-temperature superconductors. *Phys Rev Lett* 63:1996–1999.
28. Hayden SM, et al. (1991) Magnetic fluctuations in $La_{1.95}Ba_{0.05}CuO_4$. *Phys Rev Lett* 66:821.
29. Keimer B, et al. (1991) Scaling behavior of the generalized susceptibility in $La_{2-x}Sr_xCuO_{4+y}$. *Phys Rev Lett* 67:1930.
30. Aronson MC, et al. (1995) Non-Fermi liquid scaling of the magnetic response of $UCu_{5-x}Pd_x$(x=1,1.5). *Phys Rev Lett* 75:725.
31. Montfrooij W, et al. (2003) Extended versus local fluctuations in quantum critical $Ce(Ru_{1-x}Fe_x)_2Ge_2$ ($x = x_c = 0.76$). *Phys Rev Lett* 91:087202.
32. Kim MG, et al. (2015) Spin dynamics near a putative antiferromagnetic quantum critical point in Cu-substituted $BaFe_2As_2$ and its relation to high-temperature superconductivity. *Phys Rev B* 92:214404.
33. Fisher DS (1992) Random transverse field Ising spin chains. *Phys Rev Lett* 69:534–537.
34. Thill M, Huse DA (1995) Equilibrium behavior of quantum Ising spin glass. *Physica A* 214:321–355.
35. Castro Neto AH, Jones BA (2000) Non-Fermi-liquid behavior in U and Ce alloys: Criticality, disorder, dissipation, and Griffiths-McCoy singularities. *Phys Rev B* 62:14975–15011.
36. Vojta T, Schmalian J (2005) Quantum Griffiths effects in itinerant Heisenberg magnets. *Phys Rev B* 72:045438.
37. Miranda E, Dobrosavljevic V (2005) Disorder-driven non-Fermi liquid behaviour of correlated electrons. *Rep Prog Phys* 68:2337–2408.
38. Hohenberg PC, Halperin BI (1977) Theory of dynamic critical phenomena. *Rev Mod Phys* 49:435.
39. Hou C, Varma CM (2016) Phase diagram and quantum-criticality of the two dimensional dissipative quantum XY model. *Phys Rev B* 94:201101.
40. Zhu L, Hou C, Varma CM (2016) Quantum criticality in the two-dimensional dissipative quantum XY model -II. *Phys Rev B* 94:235156.
41. Haule K, Kotliar G (2009) Coherence-incoherence crossover in the normal state of iron oxypnictides and importance of Hund's rule coupling. *New J Phys* 11:025021.
42. Yin ZP, Haule K, Kotliar G (2011) Kinetic frustration and the nature of the magnetic and paramagnetic states in iron pnictides and iron chalcogenides. *Nat Mater* 10:932–935.
43. McNally DE, et al. (2014) On the origin of the charge gap in LaMnPO. *Phys Rev B* 90:180403R.
44. Matsumoto Y, et al. (2011) Quantum criticality without tuning in the mixed valence compound β–$YbAlB_4$. *Science* 331:316–319.
45. Tomita T, Kuga K, Uwatoko Y, Coleman P, Nakatsuji S (2015) Strange metal without magnetic criticality. *Science* 349:506–509.
46. Rodriguez JA, et al. (2008) MACS–A new high intensity cold neutron spectrometer at NIST. *Meas Sci Technol* 19:034023.
47. Squires GL (2012) *Introduction to the Theory of Thermal Neutron Scattering* (Cambridge Univ Press, Cambridge, UK).